



HAL
open science

Helium transport in sediment pore fluids of the Congo-Angola margin

Carine Chaduteau, Philippe Jean-Baptiste, Elise Fourré, Jean-Luc Charlou,
Jean-Pierre Donval

► **To cite this version:**

Carine Chaduteau, Philippe Jean-Baptiste, Elise Fourré, Jean-Luc Charlou, Jean-Pierre Donval. Helium transport in sediment pore fluids of the Congo-Angola margin. *Geochemistry, Geophysics, Geosystems*, 2009, 10 (1), pp.n/a-n/a. 10.1029/2007GC001897 . hal-03196755

HAL Id: hal-03196755

<https://hal.science/hal-03196755>

Submitted on 14 Apr 2021

HAL is a multi-disciplinary open access archive for the deposit and dissemination of scientific research documents, whether they are published or not. The documents may come from teaching and research institutions in France or abroad, or from public or private research centers.

L'archive ouverte pluridisciplinaire **HAL**, est destinée au dépôt et à la diffusion de documents scientifiques de niveau recherche, publiés ou non, émanant des établissements d'enseignement et de recherche français ou étrangers, des laboratoires publics ou privés.



Helium transport in sediment pore fluids of the Congo-Angola margin

Carine Chaduteau

LSCE, IPSL, Laboratoire CEA, CNRS, UVSQ, F-91191 Gif-sur-Yvette, France

Laboratoire de Géochimie et Métallogénie, IFREMER, F-29280 Plouzané, France

Philippe Jean-Baptiste and Elise Fourré

LSCE, IPSL, Laboratoire CEA, CNRS, UVSQ, F-91191 Gif-sur-Yvette, France (elise.fourre@cea.fr)

Jean-Luc Charlou and Jean-Pierre Donval

Laboratoire de Géochimie et Métallogénie, IFREMER, F-29280 Plouzané, France

[1] During the ZaiRov2 cruise of the ZaiAngo project (1998–2000) on the passive Congo-Angola margin, several gravity cores were analyzed for helium isotopic composition of sedimentary pore waters in two cold fluid seepage zones: the Astrid slide area and the Regab giant pockmark. Gas concentration and isotopic composition are presented along with thermal data in terms of the origin and circulation of fluids. Helium isotope data lie on a mixing line between bottom seawater and an almost pure radiogenic. Helium and temperature vertical profiles are well described by the classic diffusion-advection equation. On the basis of He profiles, we estimate the advection rate on the rim of the pockmark between 1.2 and 2.3 mm/a. The He flux derived for a pure diffusive regime (2.4×10^{-8} mol/m²/a) can favorably be compared to literature data and contrasts with the flux computed close to the pockmark center (1.9×10^{-7} mol/m²/a). Helium depth profiles turned to be more sensitive to advection rate than temperature profiles are.

Components: 6158 words, 10 figures, 1 table.

Keywords: helium; pockmark; pore fluids; Regab; sediment; Zaire-Angola margin.

Index Terms: 1051 Geochemistry: Sedimentary geochemistry; 3002 Marine Geology and Geophysics: Continental shelf and slope processes (4219); 3015 Marine Geology and Geophysics: Heat flow (benthic).

Received 16 November 2007; **Revised** 27 October 2008; **Accepted** 13 November 2008; **Published** 9 January 2009.

Chaduteau, C., P. Jean-Baptiste, E. Fourré, J.-L. Charlou, and J.-P. Donval (2009), Helium transport in sediment pore fluids of the Congo-Angola margin, *Geochem. Geophys. Geosyst.*, 10, Q01002, doi:10.1029/2007GC001897.

1. Introduction

[2] Continental margins are dynamic environments favoring the generation of both biogenic and thermogenic gases and fluid migration. Compaction and overpressure (like in oil reservoir leaking, aquifer freshwater expulsion, or magmatic intrusion) cause

fluids to migrate through the sedimentary column and reach the seafloor [Ballentine *et al.*, 2002; Berndt, 2005]. The consequences are shallow gas accumulations, gas or water seeps, pockmarks, mud volcanoes, or natural gas hydrates deposits, often associated with cold seep communities and methane-derived authigenic carbonates. On the

basis of these features, several authors presented an overview of fluid venting sites in marine sediments on a global scale [e.g., *Fleisher et al.*, 2001; *Judd*, 2003; *Mazurenko and Soloviev*, 2003]. A large majority of these sites are the result of focused fluid migration through sediments.

[3] ZaiAngo (1998–2000), a joint project between IFREMER and the TOTAL oil company, was dedicated to the geological and geochemical exploration of a large area of the Congo-Angola margin [*Savoie et al.*, 2000]. The research project also included the study of cold seeps and gas hydrate deposits associated with several previously identified pockmarks. Pockmarks were first observed on side scan sonar records off Nova Scotia (Canada) and described by *King and MacLean* [1970] as “cone-shaped depressions possibly formed by either ascending gas or subsurface water leakage from underlying sediments.” They usually appear in fine-grained sediments as circular depressions ranging in size from small units (1–10 m wide, <1 m deep) to larger structures ten to several hundred meter wide and up to 45 m deep [*Hovland et al.*, 2002]. *Hovland and Judd* [1988] observed that pockmarks occur all over the world and in a wide variety of geological settings. As part of the ZaiAngo project, the ZaiRov2 cruise (December 2000) on board the R/V *L'Atalante* was aimed at exploring two areas of the Lower Congo Basin: the Astrid slide, and the giant Regab pockmark. Here, we focus on helium concentration and isotopic composition in interstitial pore fluids recovered from several gravity cores and discuss the origin and circulation of fluids.

[4] The predominant source of ^4He in the Earth is from the radioactive decay of U and Th, whereas most of the ^3He is primordial in origin. Owing to their chemical inertness and contrasted composition in the various earth reservoirs, helium isotopes have been used extensively as tracers of mantle volatile inputs and provide information on fluid origin not available from the study of active chemical species [*Lupton*, 1983]. Precise measurements of helium concentrations also allow us to quantify diffusive and advective fluxes through the sediment column and to determine pore fluid advection rates [*Barnes and Clarke*, 1987; *Sayles and Jenkins*, 1982]. However, in spite of the potential of this geochemistry tool, its use in pore water studies has been hampered by the difficulties in collecting good samples (i.e., without gas loss and/or contamination problems). Here we used a new sampling and extraction method which allows

the quantitative analysis of helium isotopes [*Chaduteau et al.*, 2007].

2. Geological Setting

[5] The passive continental margin of West Africa originates from the breakup of the Gondwana supercontinent [*Rabinowitz and Labrecque*, 1979]. The rifting of South America and Africa and the opening of the South Atlantic ocean basin started at Early Cretaceous (130 Ma). The Angola margin is a nonvolcanic margin [*Contrucci et al.*, 2004]. From East to West, reflection and refraction seismic data show four different domains (Figure 1): (1) a domain with 30-km thick continental crust, (2) a domain where the crust thins from 30 km to about 5 km, (3) a transitional domain with a crust not recognized as continental or oceanic, and (4) a domain of 6-km thick oceanic crust [*Contrucci et al.*, 2004; *Moulin et al.*, 2005].

[6] The sedimentary series of the Congo-Angola basin show three main units, which correlate with three tectonic phases [*Marton et al.*, 2000]: prerift continental deposits (Jurassic), syn-rift lacustrine deposits (early Cretaceous), and postrift marine deposits (Aptian to present). Following a large accumulation of evaporites during the Aptian, the postrift stratigraphy is characterized by an aggradation of a carbonate/siliclastic ramp from Albian to Eocene, a truncation by a major erosional unconformity at Oligocene, and the progradation of a terrigenous wedge from Miocene to present [*Séranne et al.*, 1992]. This switch in marine succession was initiated independently from any tectonic forcing and can be explained by the transition from a greenhouse to an “ice house” period. During the ice house period, high-frequency sea level changes and an alternating drier and wetter climate enhanced continental weathering [*Séranne*, 1999]. The increased terrigenous input to the margin has led to the formation of the Zaïre system, a large turbiditic submarine fan directly fed by the Zaïre River and characterized by numerous turbiditic paleochannels. It extends from the base of the slope (at about 2000 m depth) to the Angola abyssal plain with a water depth of at least 5000 m, representing a total length of about 800 km [*Droz et al.*, 2003].

[7] The location of the Regab and Astrid sites is shown in Figure 2. Regab is an active giant pockmark, located at 3160 m depth in the abyssal domain less than 10 km north of the channel system of the Zaïre fan. The large size of the

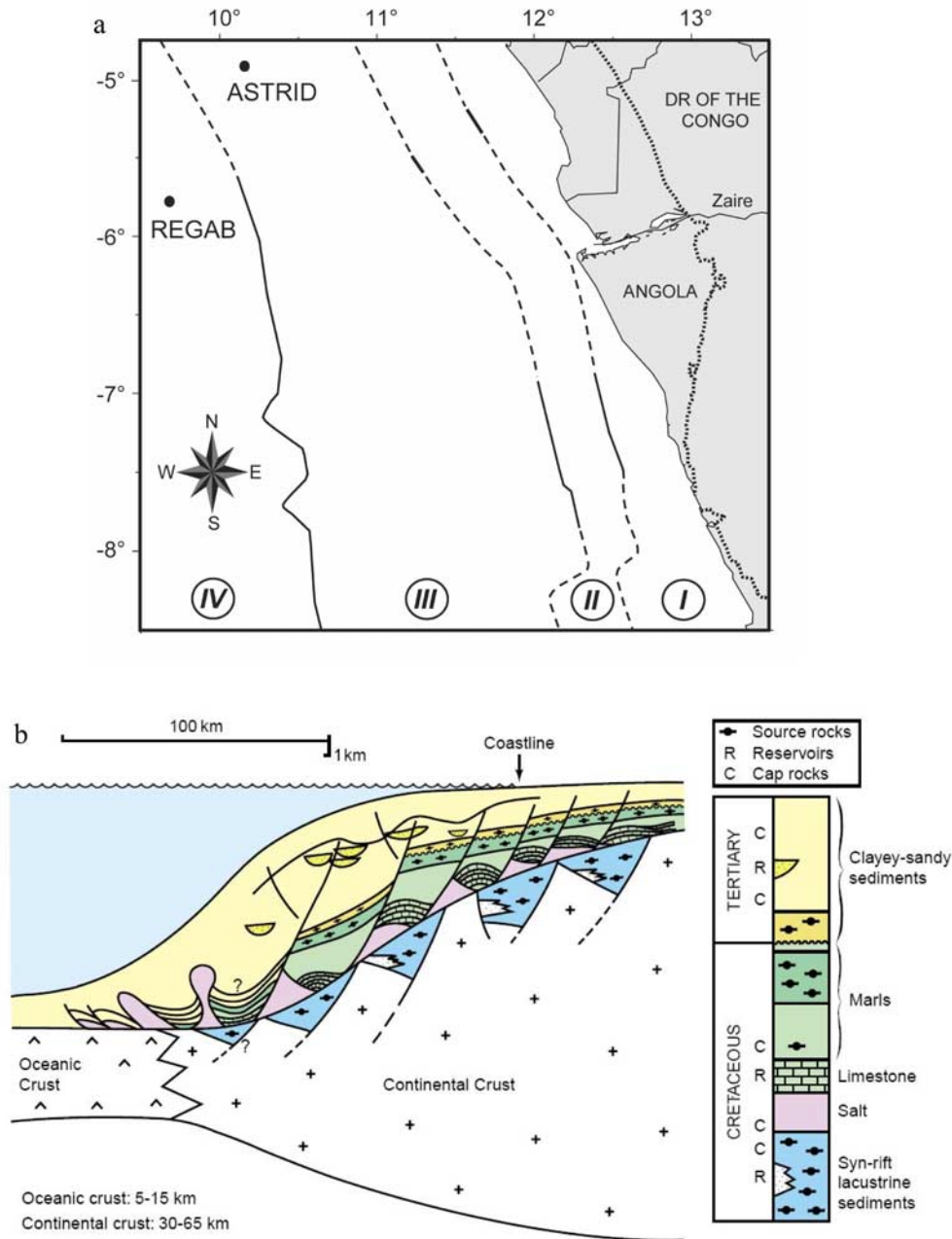


Figure 1. (a) Major structural domains of the Congo-Angola margin based on seismic and gravity data: zone I is the unthinned continental domain; zone II is the domain where the crust thins; zone III is the transitional domain; and zone IV is the oceanic domain (map adapted from *Moulin et al.* [2005]). (b) Schematic geological cross section of South Atlantic margin offshore Congo and Angola (taken from *Huc* [2004]).

pockmark, 800 m wide and 20 m deep on average, results from the collapse of a cluster of several smaller pockmarks [*Ondréas et al.*, 2005]. Gas hydrate outcrops are present on the seabed. A massive hydrate layer was also observed at 12 m below the seafloor in one core [*Charlou et al.*, 2004]. Astrid is located at 2820 m depth in the

Zaire deep-sea fan 80 km north of the channel system. It corresponds to a gravity slide area where a cluster of pockmarks is observed. Whereas Regab is in the oceanic domain, Astrid is in the transitional domain of the margin (Figure 1). According to the seismic velocity profiles of *Contrucci et al.* [2004] and *Moulin et al.* [2005], Regab is on top of

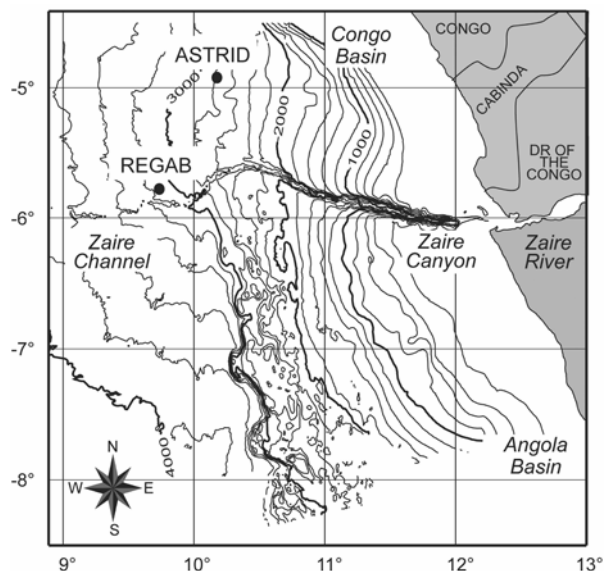


Figure 2. Location of Astrid and Regab areas on the bathymetric map of the Congo-Angola margin.

6 km of sediment and 6 km of oceanic crust while Astrid is on top of 9–10 km of sediment and 6 km of transitional crust.

3. Sampling and Methods

3.1. Core Locations

[8] Four Küllenberg cores equipped with nine thermistors outrigged onto the piston corer [Harmegnies and Landuré, 2003] were taken for gas sampling: one in the Astrid area, KZR-33 (13.65 m long), and three in the Regab area: KZR-37 (13.09 m long), KZR-38 (13.74 m long), and KZR-40 (11.93 m long). The Astrid core is located on a gravity slide headscarp. In the Regab area, KZR-37 and KZR-38 cores are located outside the pockmark, at 2 km and 1 km west of the center, respectively, whereas KZR-40 stands inside the pockmark at the western edge (Figure 3). Core recovery at the center of the pockmark was impossible due to soft sediments falling through the core catcher.

3.2. Helium Isotopes

[9] Sampling was carried out immediately following the core retrieval and its cutting into 1 m long segments and was done prior to any other core manipulation to minimize potential gas loss and atmospheric contamination. The principle of the sampling technique was to use copper tubes (1.2 cm OD, 25 cm in length) equipped with a

small piston to take minicores at both ends of each segment. The copper tube was tightly sealed with metallic clamps. Back in the laboratory, each copper tube was placed on a vacuum line and sediment was transferred into a glass bulb by applying pressurized degassed (helium-free) water at one end of the tube. Helium was then extracted from the sediment slurry using a standard method developed for water samples and analyzed by mass spectrometry with a MAP 215–50 spectrometer [Jean-Baptiste *et al.*, 1992]. The extraction blank is typically 1% of the total helium signal. The 2-sigma uncertainty in the $^3\text{He}/^4\text{He}$ ratio is about 3%. For helium concentrations, error bars are indicated in Table 1. Full details of the sampling method and analytical procedure are available in the work of Chaduteau *et al.* [2007].

3.3. Temperature Profiles

[10] Temperature profiles and heat flow determinations were obtained on all studied cores. Temperature was measured with a single-penetration probe equipped with nine thermistors. Conductivities were measured on board the ship using a needle probe technique [Von Herzen and Maxwell, 1959] with a typical spacing of ~20 cm. Heat flow was determined as the product of thermal conductivity and temperature gradient following

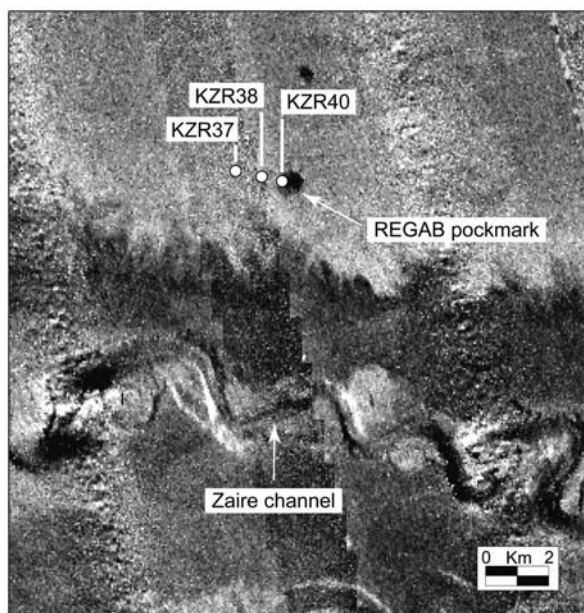


Figure 3. Location of the Regab zone on a Simrad EM-12 multibeam sonar image of the Zaire deep-sea fan.

Table 1. ^{20}Ne -Corrected Pore Fluid Helium Isotope Data^a

Sample	Depth (m)	Corrected ^4He (10^{-8} cc/g)	σ (10^{-8} cc/g)	Correction (%)	Corrected ^3He (10^{-14} cc/g)	σ (10^{-14} cc/g)	Correction (%)	^{20}Ne (10^{-7} cc/g)	Corrected R/Ra ^b
<i>KZR33- Astrid</i>									
3-4	3.99	14.17	0.27	0.6	6.15	0.24	2.00	1.65	0.31
5-6	5.99	17.88	0.29	-	6.17	0.13	-	1.56	0.25
7-8	8.01	20.62	0.49	22.5	6.38	0.44	56.50	3.49	0.22
9-10	10.01	28.33	0.49	1.0	5.86	0.25	6.60	1.71	0.15
<i>KZR37- Regab 2 km W</i>									
S-1	0.91	5.51	0.16	0.1	6.03	0.23	0.10	1.62	0.79
2-3	2.73	6.57	0.11	-	6.68	0.15	-	1.55	0.74
3-4	3.91	7.30	0.18	2.0	6.17	0.23	3.20	1.66	0.61
4-5	4.89	8.10	0.14	-	6.46	0.14	-	1.61	0.58
5-6	5.89	8.25	0.20	5.5	5.65	0.25	10.50	1.77	0.50
6-7	6.89	9.22	0.21	0.4	6.37	0.24	0.80	1.63	0.50
7-8	7.89	9.72	0.16	-	6.27	0.14	-	1.58	0.47
8-9	8.89	10.19	0.22	1.4	6.15	0.25	3.20	1.66	0.44
9-10	9.58	11.16	0.24	1.7	5.94	0.25	4.40	1.68	0.39
11-12	11.58	13.35	0.27	3.4	5.87	0.24	10.10	1.77	0.32
12-13	12.58	14.41	0.24	-	6.21	0.14	-	1.61	0.31
<i>KZR38- Regab 1 km W</i>									
1-2	2	6.83	0.19	6.5	6.08	0.25	9.80	1.77	0.64
2-3	3	8.22	0.25	0.6	6.15	0.21	1.10	1.63	0.54
4-5	5	9.28	0.22	6.6	5.32	0.23	14.60	1.83	0.42
5-6	6	10.53	0.18	-	6.43	0.15	-	-	0.44
7-8	8	12.15	0.25	1.2	6.38	0.20	3.10	1.67	0.38
8-9	9	12.72	0.26	2.4	6.15	0.20	6.60	1.72	0.35
9-10	10	14.16	0.28	1.4	6.25	0.19	4.20	1.68	0.32
10-11	11	15.44	0.29	0.8	6.36	0.20	2.60	1.66	0.30
11-12	12	17.72	0.45	-	6.74	0.15	-	1.57	0.28
<i>KZR40- Regab Inside</i>									
1-2	1.78	9.04	0.15	-	6.15	0.13	-	1.59	0.49
2-3	2.63	15.68	0.30	1.1	6.08	0.24	3.90	1.67	0.28
3-4	3.59	24.02	0.43	1.5	6.42	0.24	7.20	1.73	0.19
5-6	5.42	34.22	0.59	1.2	6.54	0.26	8.00	1.75	0.14
7-8	7.19	44.58	0.77	0.1	6.75	0.24	1.30	1.64	0.11
8-9	8.07	52.86	0.91	1.9	6.30	0.27	18.10	1.93	0.09
WOCE	-	4.12			5.90			1.62	1.03

^aConcentrations are per gram of pore water.

^bRa is the atmospheric ratio (1.38×10^{-6}).

the Bullard method [Harmegnies and Landuré, 2003].

3.4. Dating of Sediments

[11] KZR-33, KZR-37, and KZR-40 cores were run through an Avaatech X-ray fluorescence (XRF) Core Scanner [Richter et al., 2006] for Ca analysis. Although results are semiquantitative, this nondestructive technique provides rapid high-resolution records of the relative variability in elemental composition. An age model was then established from the radiocarbon dating of hand-picked foraminifera from Ca-rich levels and from the correlation of the CaCO_3 profiles of the different cores. KRZ-38 was not available for

analysis at the time of our study. Therefore, KZR-38 age model was assumed to be identical to nearby KZR-37. AMS radiocarbon analyses were performed at the LMC14 facility in Saclay (France).

4. Results

4.1. Helium Concentration and Isotopic Ratio

[12] Helium isotope results are displayed in Table 1, along with ^{20}Ne concentrations. Helium concentrations range between 5.51 and 52.86×10^{-8} ccSTP/g of pore water (i.e., between $2.46 \times$

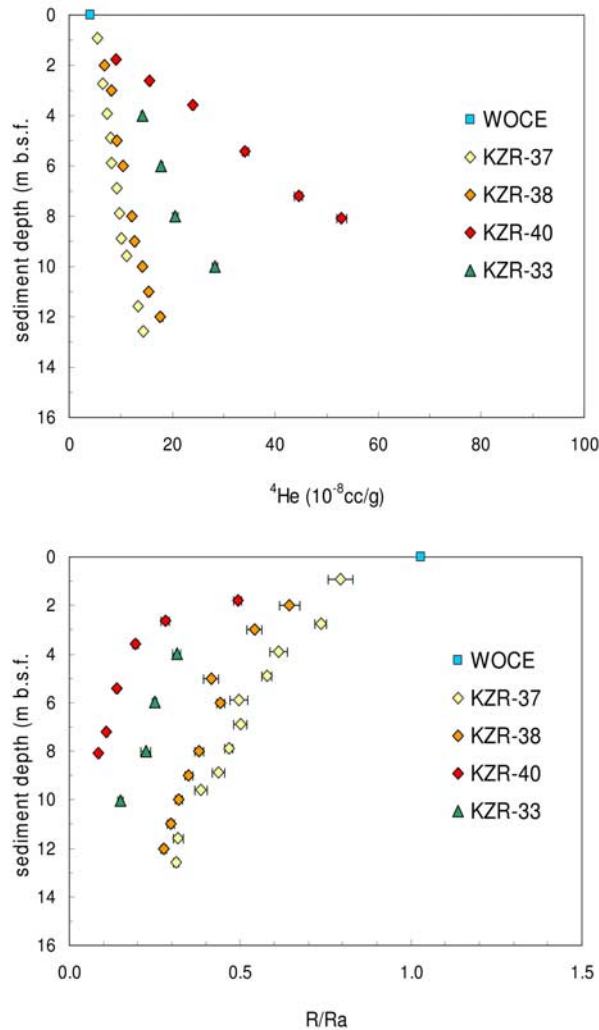


Figure 4. ^{20}Ne -corrected pore fluid helium isotope data (^4He per gram of pore water and R/R_a). When not visible, error bars are smaller than the symbols.

10^{-12} and 2.36×10^{-11} mol/g of pore water), with clearly radiogenic $^3\text{He}/^4\text{He}$ ratios between $R = 0.09$ and $R = 0.79$ Ra (where R is the $^3\text{He}/^4\text{He}$ ratio of the sample and R_a the atmospheric ratio, $R_a = 1.38 \times 10^{-6}$). The average composition of bottom waters (subscript “bw”) in the study area is available from the measurements made by the University of Bremen (<http://whpo.ucsd.edu/>) at two nearby WOCE (World Ocean Circulation Experiment) stations, A13–205 and A13–213: $^4\text{He}_{\text{bw}} = 4.12 \times 10^{-8}$ ccSTP/g (1.84×10^{-12} mol/g), $(^3\text{He}/^4\text{He})_{\text{bw}} = 1.04$ Ra, $^{20}\text{Ne}_{\text{bw}} = 1.62 \times 10^{-7}$ ccSTP/g (7.23×10^{-12} mol/g). In pore waters, neon concentrations in excess of the bottom water value are indicative of a slight atmospheric contamination (most likely due to tiny air bubble

entrapment at the surface of the copper tube during sampling) and can be used to correct the ^4He and ^3He results using the $^4\text{He}/^{20}\text{Ne}$ air ratio (0.3185) and the atmospheric $^3\text{He}/^4\text{He}$ ratio:

$$^4\text{He}_{\text{corrected}} = ^4\text{He}_{\text{measured}} - (^{20}\text{Ne}_{\text{measured}} - ^{20}\text{Ne}_{\text{bw}}) \times (^4\text{He}/^{20}\text{Ne})_{\text{air}}$$

$$^3\text{He}_{\text{corrected}} = ^3\text{He}_{\text{measured}} - (^{20}\text{Ne}_{\text{measured}} - ^{20}\text{Ne}_{\text{bw}}) \times (^4\text{He}/^{20}\text{Ne})_{\text{air}} \times (^3\text{He}/^4\text{He})_{\text{air}}$$

For most samples, the correction made to ^4He concentrations is small (between 0.5 and 2%; see Table 1). ^3He is more sensitive to any added air component (see Table 1) since ^3He concentrations, contrary to ^4He , remain close to the oceanic bottom water background throughout the sediment column.

[13] Pore water ^4He concentrations increase steadily with depth (Figure 4). The slope of the ^4He profile becomes steeper as the distance from the center of the pockmark increases. This points to a flux of helium from below, which tends to decrease away from the pockmark (see discussion below).

4.2. Temperature Profiles: Heat Flow

[14] Temperature versus penetration depth is plotted in Figure 5. The temperature profiles for the Regab cores (KZR-37, KZR-38, and KZR-40) are almost linear, apparently suggesting a heat transfer dominated by conduction. The corresponding heat flows are 41.8, 46.3, and 45.2 mWm^{-2} , respectively. For the Astrid core (KZR-33) the heat flow is higher, reaching 58.7 mWm^{-2} . Note that the temperature profile is shifted upward due to the shallower depth of this core. These results are consistent with *Lucazeau et al.* [2004] who compiled a large amount of heat flow data from the lower Congo basin. At a small scale, they observe substantial heat flow variations in connection with salt diapirs but no temperature anomaly related to fluid venting in active pockmarks could be detected. We will see in section 5.2 that this lack of any detectable thermal anomaly is consistent with the magnitude of the upward advection rates deduced from the helium vertical profiles. At the scale of the margin, the thermal trend between the oceanic domain (42 ± 3 mWm^{-2}), the transitional domain (52 ± 10 mWm^{-2}), and the continental domain (65 ± 15 mWm^{-2}) [*Lucazeau et al.*, 2004] is consistent with our own measurements for Astrid and Regab located in the transitional and

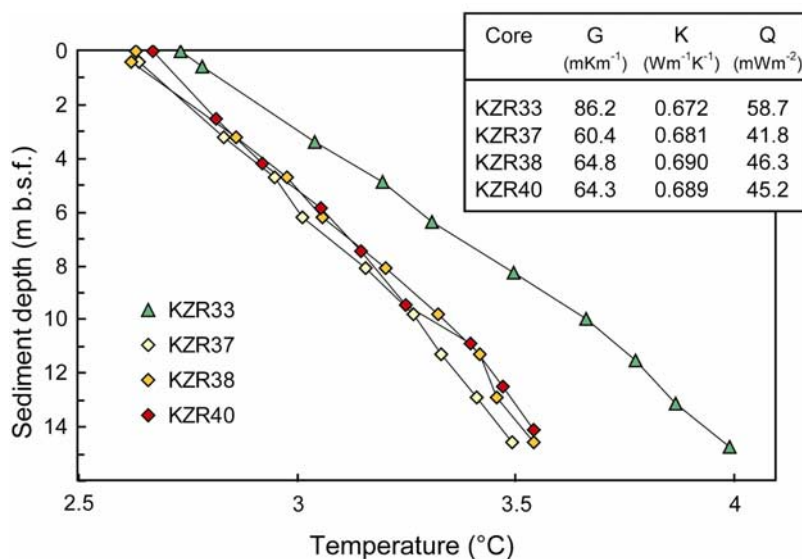


Figure 5. In situ temperature profiles and thermal data. Note that the KZR-33 profile (Astrid zone) is shifted upward due to shallower depth.

oceanic domains, respectively. These regional variations can be explained by a combination of in situ heat production in the crust and mantle heat flow: the heat production decreases offshore and is negligible in the oceanic domain, whereas mantle heat flow increases at the continent edge [Guillou and Jaupart, 1995; Lucazeau et al., 2004].

4.3. Age Model: Accumulation Rates

[15] Knowledge of the sedimentation rate is a key point in order to model fluxes. Calcium records obtained by XRF are presented in Figure 6a along with calibrated ¹⁴C ages of the Ca peaks. Comparison of the KZR-33 and KZR-37 profiles suggests that about 1 m of sediment is missing on top of core KZR-33, likely due to some landslide. Conversion of radiocarbon ages to calendar ages was done using Intcal04 [Hughen et al., 2004]. Beyond 26 cal ka BP, we relied on the new marine-derived ¹⁴C calibration of Hughen et al. [2006] which extends the calibration to ~50 ka. The age results versus depth are plotted in Figure 6b. Taking into account the 1 m that has been lost on top of KZR-33, sedimentation appears to be homogeneous over the whole area. The Holocene (13.5 ± 1.5 cm/ka) and Glacial (17 ± 2.5 cm/ka) accumulation rates are within the uncertainty of each other, and we conclude that the accumulation rate is approximately 16 ± 4 cm/ka over the whole period studied. This accumulation rate is typical of the entire period back to early Pliocene (~5 Ma)

during which about 700 m of sediment were deposited in this area [Gay et al., 2006a].

5. Discussion

5.1. Origin of Helium

[16] Helium isotope results are plotted in Figure 7 using a R/Ra versus (^{1/4}He) mixing diagram which allows to define the ³He/⁴He ratio of the helium in excess of the solubility equilibrium. For comparison, we include the few data on sediment pore waters published in the literature. All our samples fall on a simple mixing line between a bottom seawater end-member (R/Ra ~ 1; ⁴He_{bw}/⁴He = 1) and an almost pure radiogenic ⁴He source (R/Ra = 0.04). No trend is observed toward the MORB end-member (R/Ra ~ 8), as it is seen for instance in the sediment-rich hydrothermal system of the Escabana Trough. This indicates that the contribution from MORB ³He is minimal in this system and that the helium excess is overwhelmingly derived from U/Th radioactive decay in the underlying crust and sedimentary column. As shown in Figure 7, this result is comparable to what is observed in the Nankai Trough and the Japan Trench by Sano and Wakita [1985].

5.2. Fluid Circulation and Advection Rates

[17] Two-dimensional high resolution seismic profiles across the pockmark reveal a 300 m chimney-like feature (Figure 8) interpreted as an ascending movement of fluids [Ondréas et al., 2005]. On the

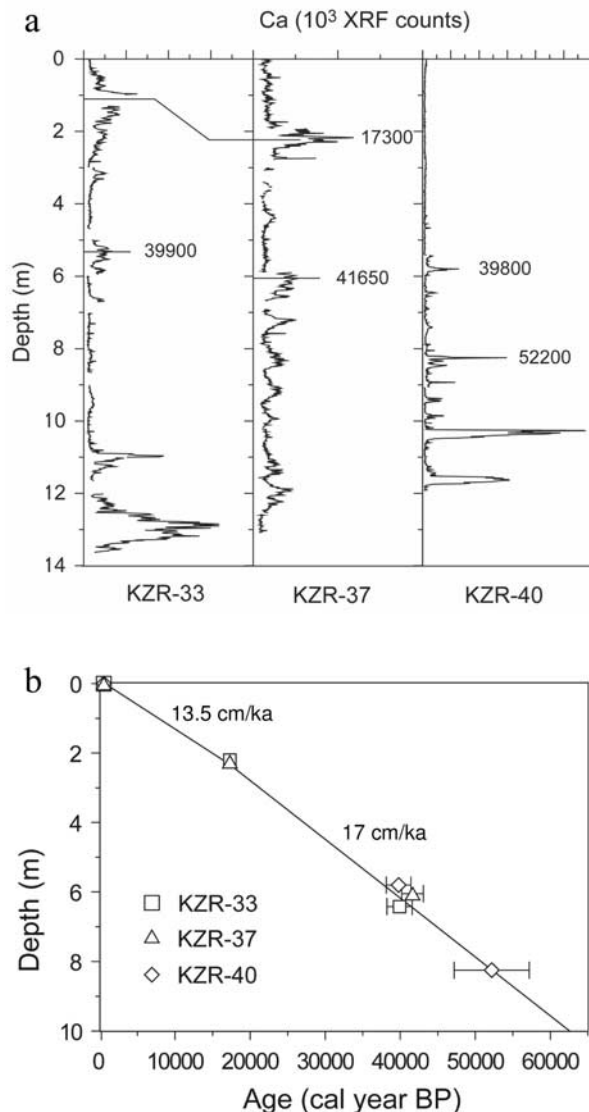


Figure 6. (a) KZR-33, KZR-37, and KZR-40 cores XRF calcium profiles. Figures are calendar ages (cal year BP) deduced from radiocarbon dating. (b) Age model for KZR-33, KZR-37, and KZR-40.

lower slope of the Congo basin, *Gay et al.* [2006a] noted that a sinuous belt of pockmarks mimics the meanders of a buried paleochannel which could act as a drain for interstitial fluids. In the Regab pockmark indeed, the chimney imaged by the seismic data branches on an ancient buried channel levee system [*Gay et al.*, 2006b]. Therefore, it seems likely that the Regab fluids originate from a shallow (~300 m) silty-sandy paleochannel reservoir from which they are expelled by the overpressure due to compaction.

[18] The helium vertical profiles for KZR-37, KZR-38, and KZR-40 are consistent with this scheme:

the three cores are close to each other, so their different slopes cannot be explained by variations in sediment thickness, ^4He diffusion, or production rate. We have also shown that sediment accumulation rates are similar for the three cores. Therefore, from KZR-37 to KZR-40, the decreasing slopes reflect an increasing fluid upward circulation when approaching the center of the pockmark. This upward velocity can be estimated by solving the helium diffusion/advection mass balance in the sediment column. To do this, we first solved the helium diffusion/advection equation numerically in the transient mode (i.e., with a growing sediment column simulating the sedimentation process) and compared the results to a simple steady state solution which neglects sediment accumulation. The results are identical, indicating that the sediment accumulation rate (~16 cm/ka) is not high enough to play a significant role in the diffusion/advection process. Hence, the profiles can be safely described by the classic steady state diffusion/advection equation (equation (1)) [*Fick*, 1855] for which an analytical solution is available:

$$D \frac{\partial C(x)}{\partial x} + C(x) \times V = J_0 \quad (1)$$

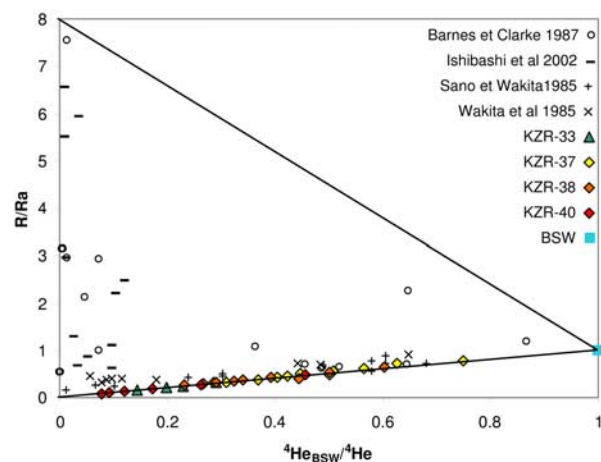


Figure 7. (R/R_a) versus ($^4\text{He}_{\text{BSW}}/^4\text{He}$) for measured sediment pore fluids. Data from the Nankai Trough and the Japan Trench [*Sano and Wakita*, 1985], from the Ontong-Java plateau and Chatham Rise [*Wakita et al.*, 1985], from the Escabana Trough [*Ishibashi et al.*, 2002], and from different ODP sites in the Pacific and the Atlantic [*Barnes and Clarke*, 1987] are shown for comparison. For *Sano and Wakita* [1985] and *Wakita et al.* [1985] for which only $^{20}\text{Ne}/^4\text{He}$ ratios are available, we use the neon solubility data of *Weiss* [1971]. The two lines represent mixing trends between bottom seawater ($R \approx R_a$) and MORB ($R \approx 8R_a$) or pure radiogenic helium sources, respectively.

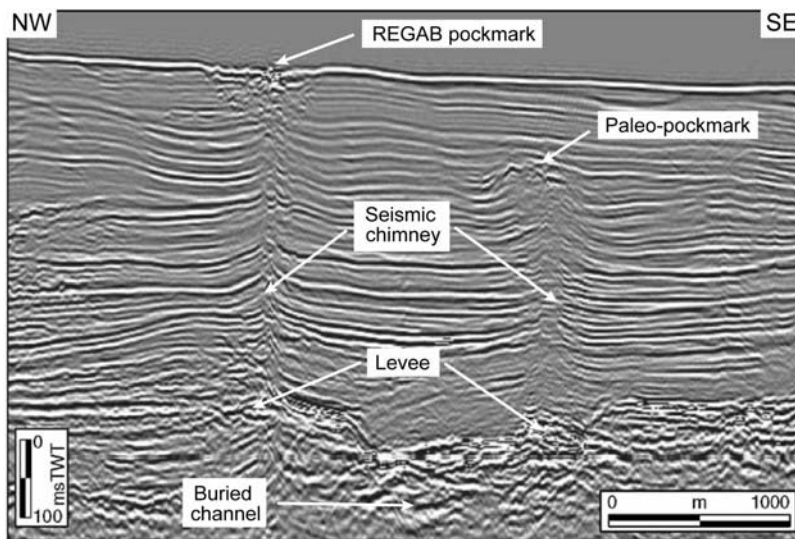


Figure 8. Two dimensional high resolution seismic profile across the Regab pockmark: the seismic chimneys are interpreted as an ascending movement of fluids from an ancient buried channel-levee system (after Gay *et al.* [2006b]).

where x is depth ($x = 0$ at the seawater/sediment interface), C is the helium concentration per volume unit of the bulk sediment (concentration in the bulk sediment equals that in pore water multiplied by the porosity n expressed as the volume of pore space per volume unit of bulk sediment), D is the He bulk diffusion coefficient, and J_0 is the helium flux through the sediment column. With this formalism, the advection velocity V is defined by $V = v/n$, where v is the volume of water advected by unit of surface area and unit of time and n is the porosity of the sediment ($n = 0.86 \pm 0.03$ from onboard measurements with Multi Sensor Core Logger). Two boundary conditions are necessary to solve this equation analytically: the first condition is that $C(0)/n$ is equal to the He concentration measured in bottom seawater. For the second condition, based on the existence of a fluid reservoir (high permeability layer) at $x = 300$ m revealed by seismic imaging [Gay *et al.*, 2006b], we choose to set a constant ^4He concentration (C_{deep}) in this paleochannel reservoir at this depth, further called H ($= 300$ m).

[19] The helium concentration as a function of depth inferred from equation (1) is thus the following:

$$\frac{C(x)}{C(0)} = \frac{\left(\frac{C_{\text{deep}}}{C(0)} - e^{-\frac{V}{D}H}\right)}{\left(1 - e^{-\frac{V}{D}H}\right)} \left(1 - e^{-\frac{V}{D}x}\right) + e^{-\frac{V}{D}x} \quad (2)$$

This analytical solution requires a constant porosity and tortuosity. In the studied zone, the variation of

these parameters with depth is unknown. To estimate this effect, we ran a finite difference numerical simulation with conservative estimates for these parameters [Briggs *et al.*, 1998; Bahr *et al.*, 2001]. A comparison of the results indicates that the analytical solution may overestimate the calculated advection rate by 15% at most.

[20] To determine the He concentration in the paleochannel reservoir at $H = 300$ m (C_{deep}), we assume a negligible advection for the KZR37 core, which leads to a concentration at depth of 2.1×10^{-6} ccSTP (9.4×10^{-11} mol) per cm^3 of bulk sediment. The best fit with the KZR40 helium profile is then obtained for a V/D value of $2.6 \times 10^{-2} \text{ m}^{-1}$ (see Figure 9). The effective diffusion coefficient D is lower than the diffusion coefficient in free water ($D_0 \sim 5 \times 10^{-9} \text{ m}^2/\text{s}$) [Jähne *et al.*, 1987] due to the tortuosity of the bulk sediment. Traditionally, D is linked to D_0 by the relation $D = D_0/(nF)$, where F is the “formation factor,” in the range 1.3 to 3 for deep-sea sediments [Boyce, 1967]. In diffusion experiments on several deep-sea sediments, Ohsumi and Horibe [1984] found typical effective diffusion coefficients for helium in superficial deep-sea sediments between 2 and $3 \times 10^{-9} \text{ m}^2/\text{s}$, in good agreement with the formation factors determined by resistivity measurements. Thus we adopt a D value of $(2.5 \pm 0.5) \times 10^{-9} \text{ m}^2/\text{s}$. It follows that advection v in the KZR40 core is in the range 1.2–2.3 mm/a. The modeled curves are included in Figure 9.

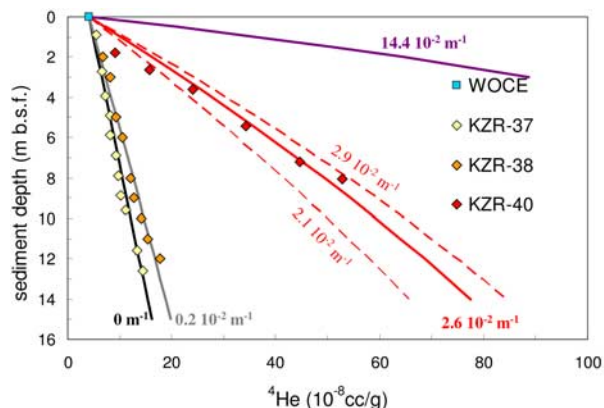


Figure 9. Neon-corrected ^4He concentrations in sediment pore fluids. Error bars are given in Table 1 (they are of the size of the symbols for KZR37 and 38 and slightly larger for KZR 40). Solid curves correspond to the analytical solution of the steady state advection-diffusion equation (see text) for various V/D values (see figures on the curves). For $D = 2.5 \times 10^{-9} \text{ m}^2/\text{s}$ (see text), the purple curve corresponds to a 10 mm/a advection, the solid red curve to 1.8 mm/a (the dashed red curves to 1.45 and 2.01 mm/a, respectively), and the gray curve to 0.1 mm/a.

[21] The He flux in the pure diffusive regime is deduced from KZR37 profile: $2.4 \times 10^{-8} \text{ mol/m}^2/\text{a}$. This value supports the oceanic crustal flux estimated by *Torgersen* [1989] from the production rate: he obtained a lower limit of $1.73 \times 10^{-8} \text{ mol/m}^2/\text{a}$ (considering 400 m of 80% carbonated sediment on top of the crust) and an upper limit of $9.4 \times 10^{-8} \text{ mol/m}^2/\text{a}$. It is also consistent with the few data derived from sediment measurements we found in the literature: $[0.6-3.3] \times 10^{-8} \text{ mol/m}^2/\text{a}$ [*Barnes and Bieri*, 1976] and $[0.1-2.1] \times 10^{-8} \text{ mol/m}^2/\text{a}$ [*Sano and Wakita*, 1987]. More recently, *Well et al.* [2001] derived an average flux of $(5.2 \pm 2) \times 10^{-8} \text{ mol/m}^2/\text{a}$ from the helium excess in Pacific deep waters.

[22] For KZR40, the best estimate of V/D ($2.6 \times 10^{-2} \text{ m}^{-1}$) corresponds to a flux of $1.9 \times 10^{-7} \text{ mol/m}^2/\text{a}$. This value is an order of magnitude higher than that of the pure diffusive regime, illustrating the focusing effect of the pockmark. In comparison, the ^4He in situ production can be estimated to $1.2 \times 10^{-9} \text{ mol/m}^2/\text{a}$ using a typical crustal composition for the mineral fraction of the sediment ($U = 1 \text{ ppm}$ and $\text{Th}/U = 4$) and is in fact negligible.

[23] An advection rate of the order of a few mm/a is not in contradiction with the temperature data, even if at first sight the similarity of the temperature profiles between KZR-37, KZR-38, and KZR-40 would suggest a purely conductive heat transfer

for all the cores. In fact the same type of diffusion/advection equation can be solved for heat. The simulated temperature profiles for different advection rates are plotted in Figure 10. It shows that temperature profiles are far less sensitive to advection than He profiles and that an increase of advection between KZR-37 and KZR-40 is not inconsistent despite similarities between the two temperature profiles. This is due to the thermal diffusion coefficient ($\sim 1.7 \times 10^{-7} \text{ m}^2/\text{s}$) being almost two orders of magnitude higher than the He diffusion coefficient. Hence, helium is clearly a more sensitive tracer of fluid movements in the sediment column.

[24] The KZR-33 helium profile, located in the Astrid zone, lies in an intermediate position (Figure 7). Whether this profile is influenced by advection (since the Astrid site is a cluster of pockmarks) or by a higher flux linked to the greater heat flux from the continental crust due to its geographical position closer to the continental domain is difficult to say. As a matter of fact we lack the appropriate geophysical data to set realistic lower boundary conditions that would allow us to test both hypotheses.

6. Conclusions

[25] We measured helium and methane vertical concentration profiles in sediment pore waters from two cold fluid seepage zones of the Congo-Angola margin: the Astrid slide area and the Regab giant pockmark. For helium, we used a new method for gas sampling and recovery which avoids the long-standing gas loss and/or air contamination problems classically associated with pore water sampling. The main results of the present study are the following:

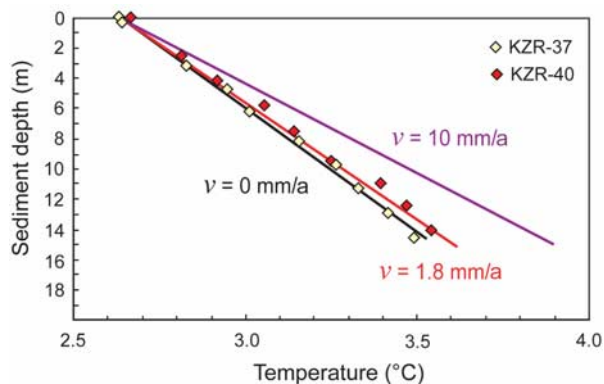


Figure 10. Comparison between measured and modeled temperature profiles using the same type of boundary conditions as for helium.

[26] 1. Sedimentation is homogeneous over the whole Regab area, with an accumulation rate of 16 ± 4 cm/ka.

[27] 2. In the Astrid area, heat flow (58.7 mWm^{-2}) is slightly larger than in the Regab zone ($44.4 \pm 2.3 \text{ mWm}^{-2}$) in agreement with their geographical position with respect to the transition between the continental and oceanic domains.

[28] 3. Helium isotopes data lie on a mixing line between bottom seawater and a radiogenic, showing that the helium signature is overprinted by the ^4He production from U/Th radioactive decay in the sediment column and underlying crust.

[29] 4. Helium and temperature vertical profiles are well described by the classic steady state diffusion-advection equation. In the Regab zone where three different cores could be compared, helium profiles show increasing advection rates toward the center of the pockmark For core KZR40 located inside the pockmark, we calculate an advection rate in the range 1.2–2.3 mm/a.

[30] 5. The derived He flux is $2.4 \times 10^{-8} \text{ mol/m}^2/\text{a}$ for the pure diffusive regime (KZR37) which is in good agreement with both estimations computed from He production rate [Torgersen, 1989] and from experimental measurements [Barnes and Bieri, 1976; Sano and Wakita, 1987; Well et al., 2001]. For the core closest to the pockmark center (KZR40), the flux is estimated to $1.9 \times 10^{-7} \text{ mol/m}^2/\text{a}$, an order of magnitude higher than for KZR37, illustrating the focusing effect of the pockmark.

[31] 6. Comparison between helium and thermal profiles shows that helium is a far more sensitive tracer of water movements than temperature.

Acknowledgments

[32] The ZaiRov2 cruise was funded through the ZAIANGO project of cooperation between TOTAL and IFREMER. We thank the captain, officers, and crew of the R/V *L'Atalante* and the ROV *Victor* staff who made the Zairov2 scientific cruise a success. We are grateful to Hélène Ondréas the chief scientist, Gilbert Floch for the core handling, François Harmegnies for the in situ sediment temperature measurements, and Henri Bougault who inspired this work and collected the helium samples. We thank Evelyne Cottureau for the radiocarbon data. We also wish to thank J. Ishibashi, G. Snyder, and A. Battani for their helpful comments on the manuscript.

References

Bahr, D. B., E. Hutton, J. Syvitski, and L. Pratson (2001), Exponential approximations to compacted sediment porosity

- profiles, *Comput. Geosci.*, *27*, 691–700, doi:10.1016/S0098-3004(00)00140-0.
- Ballentine, C. J., R. Burgess, and B. Marty (2002), Tracing fluid origin, transport and interaction in the crust, *Rev. Mineral. Geochem.*, *47*, 539–614, doi:10.2138/rmg.2002.47.13.
- Barnes, R. O., and R. H. Bieri (1976), Helium flux through marine sediments of the northeast Pacific Ocean, *Earth Planet. Sci. Lett.*, *28*, 331–336, doi:10.1016/0012-821X(76)90194-1.
- Barnes, R. O., and W. B. Clarke (1987), Fluids kinematics, fluid residence times, and rock degassing in oceanic crust determined from noble gases contents of Deep Sea Drilling Project pore waters, *J. Geophys. Res.*, *92*, 12,491–12,506, doi:10.1029/JB092iB12p12491.
- Berndt, C. (2005), Focused fluid flow in passive continental margins, *Philos. Trans. R. Soc. London, Ser. A.*, *363*, 2855–2871, doi:10.1098/rsta.2005.1666.
- Boyce, R. E. (1967), Electrical resistivity of modern marine sediments from the Bering Sea, *Tech. Publ. 6*, Nav. Undersea Warfare Cent., Newport, R. I.
- Briggs, K. B., P. Jackson, R. Holyer, R. Flint, J. C. Sandidge, and D. Young (1998), Two-dimensional variability in porosity, density, and electrical resistivity of Eckernförde Bay sediment, *Cont. Shelf Res.*, *18*, 1939–1964, doi:10.1016/S0278-4343(98)00064-8.
- Chaduteau, C., E. Fourré, P. Jean-Baptiste, A. Dapoiny, D. Baumier, and J. L. Charlou (2007), A new method for quantitative analysis of helium isotopes in sediment pore-waters, *Limnol. Oceanogr. Methods*, *5*, 425–432.
- Charlou, J. L., et al. (2004), Physical and chemical characterization of gas hydrates and associated methane plumes in the Congo-Angola Basin, *Chem. Geol.*, *205*, 405–425.
- Contrucci, I., L. Matias, M. Moulin, L. Géli, F. Klingelhofer, H. Nouzé, D. Aslanian, J. L. Olivet, J. P. Réhault, and J. C. Sibuet (2004), Deep structure of the West African continental margin (Congo, Zaïre, Angola), between 5°S and 8°S, from reflection/refraction seismics and gravity data, *Geophys. J. Int.*, *158*, 529–553, doi:10.1111/j.1365-246X.2004.02303.x.
- Droz, L., T. Marsset, H. Ondréas, M. Lopez, B. Savoye, and F. L. Spy-Anderson (2003), Architecture of an active mud-rich turbidite system: The Zaire Fan (Congo-Angola margin southeast Atlantic): Results from Zaiango 1 and 2 cruises, *AAPG Bull.*, *87*(7), 1145–1168, doi:10.1306/03070300013.
- Fick, A. E. (1855), On liquid diffusion, *Philos. Mag.*, *4*(10), 30–39.
- Fleisher, P., T. H. Orsi, M. D. Richardson, and A. L. Anderson (2001), Distribution of free gas in marine sediments: A global overview, *Geo Mar. Lett.*, *21*, 103–122, doi:10.1007/s003670100072.
- Gay, A., M. Lopez, P. Cochonat, D. Levaché, G. Sermondadaz, and M. Seranne (2006a), Evidences of early to late fluid migration from an upper Miocene turbiditic channel revealed by 3D seismic coupled to geochemical sampling within sea-floor pockmarks, Lower Congo Basin, *Mar. Pet. Geol.*, *23*, 387–399, doi:10.1016/j.marpetgeo.2006.02.004.
- Gay, A., M. Lopez, H. Ondreas, J. L. Charlou, G. Sermondadaz, and P. Cochonat (2006b), Seafloor facies related to upward methane flux within a Giant Pockmark of the Lower Congo Basin, *Mar. Geol.*, *226*, 81–95, doi:10.1016/j.margeo.2005.09.011.
- Guillou, C., and C. Jaupart (1995), On the effect of continent on mantle convection, *J. Geophys. Res.*, *100*, 24,217–24,238, doi:10.1029/95JB02518.
- Harmegnies, F., and J. Y. Landuré (2003), Mesures de flux thermique, ZaiAngo final report, IFREMER, Brest, France.

- Hovland, M., and A. G. Judd (1988), *Seabed Pockmarks and Seepages: Impact on Geology, Biology and the Marine Environment*, 293 pp., Graham and Trotman, London.
- Hovland, M., J. V. Gardner, and A. Judd (2002), The significance of pockmarks to understanding fluid flow processes and geohazards, *Geofluids*, *2*, 127–136, doi:10.1046/j.1468-8123.2002.00028.x.
- Huc, A. Y. (2004), Petroleum in the South Atlantic, *Oil Gas Sci. Technol.*, *59*(3), 243–253.
- Hughen, K., et al. (2004), Marine04 marine radiocarbon age calibration, 0–26 cal kyr BP, *Radiocarbon*, *46*, 1059–1086.
- Hughen, K., J. Southon, S. Lehman, C. Bertrand, and J. Turnbull (2006), Marine-derived ¹⁴C calibration and activity record for the past 50,000 years updated from the Cariaco Basin, *Quat. Sci. Rev.*, *25*, 3216–3227, doi:10.1016/j.quascirev.2006.03.014.
- Ishibashi, J., M. Sato, Y. Sano, H. Wakita, T. Gamo, and W. C. Shanks, III (2002), Helium and carbon gas geochemistry of pore fluids from the sediment-rich hydrothermal system in Escanaba Trough, *Appl. Geochem.*, *17*, 1457–1466, doi:10.1016/S0883-2927(02)00112-9.
- Jähne, B., G. Heinz, and W. Dietrich (1987), Measurement of the diffusion coefficients of sparingly soluble gases in water, *J. Geophys. Res.*, *92*, 10,767–10,776, doi:10.1029/JC092iC10p10767.
- Jean-Baptiste, P., F. Mantsi, A. Dapigny, and M. Stievenard (1992), Design and performance of a mass spectrometric facility for measuring helium isotopes in natural waters and for low level tritium determination by the ³He ingrowth method, *Int. J. Radiat. Appl. Instrum.*, *43*(7), 881–891(Part A), doi:10.1016/0883-2889(92)90150-D.
- Judd, A. G. (2003), The global importance and context of methane escape from the seabed, *Geo Mar. Lett.*, *23*, 147–154, doi:10.1007/s00367-003-0136-z.
- King, L. H., and B. MacLean (1970), Pockmarks on the Scotian Shelf, *Geol. Soc. Am. Bull.*, *81*, 3141–3148, doi:10.1130/0016-7606(1970)81[3141:POTSS]2.0.CO;2.
- Lucazeau, F., F. Brigaud, and J. L. Bouroulec (2004), High-resolution heat flow density in the lower Congo basin, *Geochem. Geophys. Geosyst.*, *5*, Q03001, doi:10.1029/2003GC000644.
- Lupton, J. E. (1983), Terrestrial inert gases: Isotope tracer studies and clues to primordial components in the mantle, *Annu. Rev. Earth Planet. Sci.*, *11*, 371–414, doi:10.1146/annurev.ea.11.050183.002103.
- Marton, L. G., G. C. Tari, and C. T. Lehmann (2000), Evolution of the Angolan passive margin, West Africa, with emphasis on post-salt structural styles, in *Atlantic Rifts and Continental Margins*, *Geophys. Monogr. Ser.*, vol. 115, edited by W. Mohriak and M. Talwani, pp. 129–149, AGU, Washington, D. C.
- Mazurenko, L. L., and V. A. Soloviev (2003), Worldwide distribution of deep-water fluid venting and potential occurrences of gas hydrate accumulations, *Geo Mar. Lett.*, *23*, 162–176, doi:10.1007/s00367-003-0146-x.
- Moulin, M., D. Aslanian, J. L. Olivet, I. Contrucci, L. Matias, L. Geli, F. Klingelhofer, H. Nouzé, J. P. Réhault, and P. Untermeier (2005), Geological constraints on the evolution of the Angolan margin based on reflection and refraction seismic data (ZaiAngo project), *Geophys. J. Int.*, *162*, 793–810, doi:10.1111/j.1365-246X.2005.02668.x.
- Ohsumi, T., and Y. Horibe (1984), Diffusivity of He and Ar in deep-sea sediments, *Earth Planet. Sci. Lett.*, *70*, 61–68, doi:10.1016/0012-821X(84)90209-7.
- Ondréas, H., et al. (2005), ROV study of a giant pockmark on the Gabon continental margin, *Geo Mar. Lett.*, *25*, 281–292, doi:10.1007/s00367-005-0213-6.
- Rabinowitz, P. D., and J. Labrecque (1979), The Mesozoic south Atlantic Ocean and evolution of its continental margins, *J. Geophys. Res.*, *84*, 5973–6002, doi:10.1029/JB084iB11p05973.
- Richter, T. O., S. Van der Gaast, B. Koster, A. Vaars, R. Gieles, H. C. De Stiegter, H. de Haas, and T. C. E. Van Weering (2006), The Avaatech XRF Core Scanner: Technical description and applications to NE Atlantic sediments, in *New Techniques in Sediment Core Analysis*, edited by R. G. Rothwell, *Geol. Soc. London Spec. Publ.*, *267*, 39–50.
- Sano, Y., and H. Wakita (1985), ³He/⁴He ratios of pore gases in pore waters, sites 583 and 584, *Init. Rep. Deep Sea Drill. Proj.*, *87*, 861–864.
- Sano, Y., and H. Wakita (1987), Helium isotopes and heat flow on the ocean floor, *Chem. Geol.*, *66*, 217–226.
- Savoie, B., et al. (2000), Structure et évolution récente de l'éventail turbiditique du Zaïre: Premier résultats scientifiques des missions d'exploration Zaïango 1 et 2 (marge Congo–Angola), *C. R. Acad. Sci., Ser. Ila Sci. Terre Planetes*, *331*, 211–220.
- Sayles, F. L., and W. J. Jenkins (1982), Advection of pore fluids through sediments in the Equatorial East Pacific, *Science*, *217*, 245–248, doi:10.1126/science.217.4556.245.
- Séranne, M. (1999), Early Oligocene stratigraphic turnover on the west Africa continental margin: A signature of the Tertiary greenhouse-to-icehouse transition?, *Terra Nova*, *11*, 135–140, doi:10.1046/j.1365-3121.1999.00246.x.
- Séranne, M., M. Seguret, and M. Fauchier (1992), Seismic super-units and post-rift evolution of the continental passive margin of southern Gabon, *Bull. Soc. Geol. Fr.*, *163*(2), 135–146.
- Torgersen, T. (1989), Terrestrial helium degassing fluxes and the atmospheric helium budget: Implications with respect to the degassing processes of continental crust, *Chem. Geol.*, *79*, 1–14.
- Von Herzen, R. P., and A. E. Maxwell (1959), The measurement of thermal conductivities of thermal conductivity of deep-sea sediments by a needle probe method, *J. Geophys. Res.*, *64*, 1557–1563, doi:10.1029/JZ064i010p01557.
- Wakita, H., Y. Sano, N. Fujii, and A. Takeuchi (1985), ³He/⁴He ratios of pore gases in deep-sea sediments, legs 89 and 90, *Init. Rep. Deep Sea Drill. Proj.*, *90*, 1261–1263.
- Weiss, R. F. (1971), Solubility of helium and neon in water and seawater, *J. Chem. Eng. Data*, *16*, 235–241, doi:10.1021/je60049a019.
- Well, R., J. Lupton, and W. Roether (2001), Crustal helium in deep Pacific waters, *J. Geophys. Res.*, *106*, 14,165–14,177, doi:10.1029/1999JC000279.